NJC

Accepted Manuscript

ROYAL SOCIETY OF CHEMISTRY

www.rsc.org/njc

Self-assembly of polyoxometalate-cholesterol conjugate into microrods or nanoribbons regulated by thermodynamics†

Hai-Kuan Yang,*,[a,b] Li-Jun Ren,[c] Han Wu[c] and Wei Wang*,[c]

[a]Department of Chemistry, North University of China, Taiyuan, Shanxi 030051, China. E-mail: haikuanyang@nuc.edu.cn

[b]Key Laboratory of Advanced Energy Materials Chemistry (Ministry of Education), Nankai University, Tianjin 300071, China

[c]Center for Synthetic Soft Materials, Key Laboratory of Functional Polymer Materials of Ministry of Education and Institute of Polymer Chemistry, and Collaborative Innovation Center of Chemical Science and Engineering (Tianjin), Nankai University, Tianjin 300071, China. E-mail: weiwang@nankai.edu.cn

† Electronic supplementary information (ESI) available: details of experimental section and additional characterizations.

Abstract: We report the self-assembly of the polyoxometalate-organic conjugate can be well controlled and regulated by means of temperature-mediated approach. The conjugate comprised of an organically modified Anderson-type polyoxometalate cluster with two cholesterol moieties, considering the symmetrical and rigid structure of Anderson-type polyoxometalate cluster is an excellent building block for constructing functional supramolecular assemblies, and cholesterol is widely explored to fabricate desired

self-assemblies, due to its planar structure together with the van der Waals interactions between molecules. Utilizing the temperature-mediated approach, the conjugate assembled into micrometre scale crystalline rods at 40.0 ^{O}C, and an organogel at 20.0 ^{O}C, in mixed DMF/toluene solvents (v/v = 1:9). For crystalline rods, they were constituted with a lot of ultralong and rigid microrods, and for organogel, it was immobilized by massive short and elongated nanoribbons. Moreover, a mechanism has been proposed to explain the self-assembly behavior of the conjugate at different temperature. This temperature-mediated approach may provide a feasible method for the fabrication of nanostructural materials for various applications.

Introduction

Controlling the self-assembly of molecules into ordered nano- and microstructures is a powerful methodology for creating novelly hard or soft materials with various properties, and has drawn considerable attention over the past decades in the field of nanoscience and nanotechnology.[1-4] In a typically molecular self-assembly process, the non-covalent interactions, such as electrostatic adsorption, hydrogen bonding, π–π stacking, and van der Waals interactions, lead small molecules to interconnect with each other to form ordered and complex molecular architectures.[5-9] Based on this strategy, a variety of well-defined materials constructed by means of supramolecular self-assembly show uniquely controllable structures, including ribbons, tubes, and rods, which give them special functional applications in the areas of liquid crystallines,[10,11] bionanotechnology,[12] functionalized soft materials,[13] and photoswitching devices.[14,15]

Polyoxometalates (POMs), an important class of structurally well-defined anionic metal-oxygen clusters of early transition metals in the highest oxidation states, are usually employed as unique primary building for controlled self-assemblies to achieve organic-inorganic hybrids or complexes by connecting covalently or noncovalently with organic components.[16-19] Controllable self-assemblies of POM-based organic-inorganic hybrids or complexes have also received much attentions recently, because of their unique supramolecular architectures and versatile functional applications in chemical field as catalysts,[20,21] liquid crystallines,[22] functional soft materials,[23] and in many other fields such as magnetics,[24] physics,[25] and biomedicines.[26-28]

The controllable self-assemblies of POM-based organic-inorganic hybrids or complexes are significantly influenced by various conditions, mainly including the structure of the organic moieties conjugated POM cluster, surfactant-enwrapped counter cations, size and structure of POM cluster, type and nature of solvents, as well as temperature. So far, many efforts have been made to realize the controllable self-assemblies of POM-based organic-inorganic hybrids. To reach the controllable self-assembly, the most widely adopted strategy is to rationally choose and design the organic moieties conjugated POM cluster at the molecular level. Until now, a large number of organic functional groups, such as aromatic groups,[29,30] photoisomerizable groups,[31,32] recognition groups,[33,34] ferrocene,[35,36] alkyl chains,[37,38] porphyrin,[39,40] dendrimers,[41-43] and polyhedral oligomeric silsesquioxane[44,45] have been connected onto POM cluster, leading to promising organic-inorganic hybrids with wonderful and controllable self-assembly. Another common strategy is to change the counter cations on POM surfaces, to offer efficiently controlled self-assembly processes. Based on

this approach, different architectures, such as nanofibers,[46,47] vesicles,[48] nanoparticles,[49,50] nanocones and nanotubes[51] have been assembled. In addition, the approach of mediating environmental conditions (*e.g.* pH valve,[52] polarity of solvent,[53] temperature,[54] optical and redox stimulus[31,36]), as a promising strategy, is considerably attractive, because it is a flexible and versatile method to fabricate the controlled organic-inorganic hybrid structures. Until now, despite massive architectures of supramolecular assemblies have been fabricated by different strategies, only a few of them were found by rational design rather than serendipity. Thus, it is still challenging to carry out novel high-controllable self-assemblies of POM-based hybrids or complexes.

Considering the influence factor of supramolecular assemblies based on POM-organic hybrids or complexes, mediating environmental conditions offers a very nice method for producing versatile architectures from simple regulation and control. In our recent study, we have been detailly studied the gelation process of the POM-cholesterol conjugate in the mixed solvents of different toluene/DMF volume fraction.[53] We found that different supramolecular structures, such as rigid and straight ribbons or twisted ribbons, were fabricated by controlling the volume fraction of the mixed solvents. In the solvent-mediated process, the non-covalent interactions (*e.g.* gelator–gelator interactions, gelator–solvent interactions) were utilized to adjust the assembled structures. The results showed that controllable self-assembled structures were constructed by adjusting the non-covalent interactions through a simple solvent-mediated approach. To investigate the self-assembly process in a straightforward way, we will perform an in-depth understanding of the POM-based self-assembly behavior by means of temperature-mediated approach in the

present work. For high-controllable morphologies of supramolecular assemblies, the

organically modied Anderson-type POM cluster and cholesterol moiety were introduced to

form the POM-cholesterol conjugate. The Anderson-type POM cluster is considered as an

excellent building block for constructing functional supramolecular assemblies because of its

symmetrical and rigid structure.[55] Meanwhile, cholesterol is widely explored to fabricate

desired self-assemblies, due to its planar structure together with the van der Waals

interactions between molecules. Considering the non-covalent interactions (*e.g.*

conjugate–conjugate interactions, conjugate–solvent interactions) between POM-cholesterol

conjugates and solvents, we expected that modulating the temperature of self-assemblies

could be a more attractive approach, which could carry out novel high-controllable

self-assemblies. Beyond that, the results will provide a deeper understanding of the control

mechanism of supramolecular assemblies.
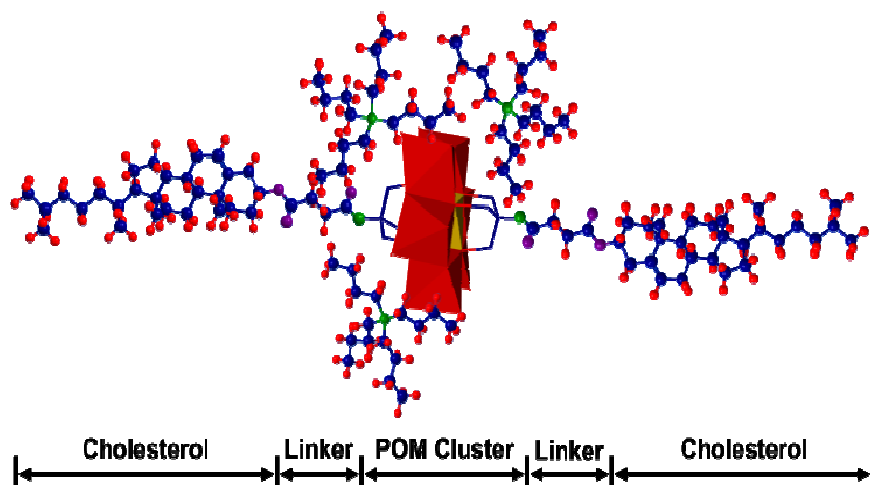
Scheme 1 Chemical structure of the POM-cholesterol conjugate.

Experimental

Materials

The details of its synthetic procedure of the POM-cholesterol conjugate have been reported in our previous study[56] and it can be seen in the ESI. The solvents are analytical grade *N,N*-dimethylformamide (DMF) and toluene, which were dried and distilled prior to use.

Preparation of POM-based gels

Typically, a known weight of the POM-cholesterol conjugate and a measured solvents of DMF/toluene were placed into the screw-cap vials and the system was heated until the solid was dissolved. Then, the sealed vial was placed into an oven, of which temperature was 60.0 ^{O}C. The vial was cooled to 20.0 ^{O}C at the rate of about 15.0 ^{O}C h^{-1}. After staying for several hours in the oven, the solutions became immobilized.

Preparation of POM-based crystalline rods

Typically, a known weight of the POM-cholesterol conjugate and a measured solvents of DMF/toluene volume fraction were placed into the screw-cap vials and the system was heated until the solid was dissolved. Then, the sealed vial was placed into an oven, of which temperature was 60.0 ^{O}C. The vial was cooled to 40.0 ^{O}C at the rate of about 15.0 ^{O}C h^{-1}. After staying for a few weeks in the oven, micrometre scale crystalline rods were acquired.

Techniques

Transmission electron microscopy (TEM), and energy-dispersive X-ray spectroscopy (EDX) were carried on a field emission transmission electron microscopy (FEI Tecnai G2 F20) operating at an acceleration voltage of 200 kV. Scanning electron microscopy (SEM) images were taken on a field emission scanning electron microscopy (JSM-6301F) operating at an

acceleration voltage of 30 kV. Fourier transformation infrared spectra (FT-IR) were recorded on a FT-IR spectrometer (Bio-Rad FTS-135) using the KBr pellet technique. Temperature-dependent fourier transformation infrared spectra (Temperature-dependent FT-IR) were recorded on a FT-IR spectrometer (Bio-Rad FTS-135) using the KBr pellet technique, and the heating runs were done stepwise (heating rate 10 K/min) from 20 to 160 ^{O}C. Thermogravimetric analysis (TGA) data were collected on Netzsch STA449F3 under argon with a rate of 10 ^{O}C /min in the range of 25 – 900 ^{O}C. The powder X-ray diffration (XRD) experiment was performed on a Rigaku D/Max-2500 X-ray diffractometer, equipped with a Cu-Ka radiation (λ = 0.154 nm) source operated at 40 kV and 100 mA at room temperature. Atomic force microscopy (AFM) images were recorded on a multi-model atomic force microscope (Digital Instrumental Nanoscope IV) using glass slide as substrate at room temperature performed in tapping mode. Optical microscopy (OM) measurements were performed with an Olympus BX-51 microscope.

Results and discussion

Preparation of the POM-cholesterol conjugate

Chemical structure of the POM-cholesterol conjugate was shown in Scheme 1. The conjugate was prepared by *o*-succinyl-cholesterol and organically functionalized POM cluster $(Bu_4N^+)_3\{(MnMo_6O_{18})^{3-}[(OCH_2)_3CNH_2]_2\}$, and details of the synthesis and characterization can be found in the ESI.

Table 1 Self-assembly behavior of the POM-cholesterol conjugate (c = 15 mg mL^{-1}) in mixed DMF/toluene solvents at 40.0 ^{O}C^{a}.

DMF/Toluene (v/v%)	State	DMF/Toluene (v/v%)	State
1:0	S	1:7	C
1:1	S	1:8	C
1:2	S	1:9	C
1:3	S	1:10	C
1:4	S	1:11	G
1:5	S	1:12	G
1:6	C	0:1	G
^{a}S = solution; C = crystal; G = gel.			

Self-assembly behavior of the POM-cholesterol conjugate

To evaluate the influence of temperature on the self-assembly behavior, the POM-cholesterol conjugate was examined in the DMF/toluene mixed solvents by altering the volume fraction and temperature. Herein, the sample was mixed with the DMF/toluene solvents of different volume fraction in the screw-cap vial and slowly heated till the sample was dissolved, then, the resulting solution was kept at different temperature for several days. Based on experiments, we found an interesting phenomenon that is the sample could form solutions, organogels, or crystal rods under the experimental conditions. In a typically experimental conditions, at c = 15 mg mL^{-1} and 40.0 ^{O}C, it can be seen that the sample was well soluble (v/v ≥ 1:5), crystalline (1:6 ≥ v/v ≥ 1:10), and gelatinous (v/v ≤ 1:11) in the DMF/toluene solvents, respectively, as summarized in Table 1. However, at c = 15 mg mL^{-1} and 20.0 ^{O}C, the sample formed good organogels only in mixed DMF/toluene solvents (v/v ≤ 1:6), but solutions in other volume fraction (see Table S1, ESI†).
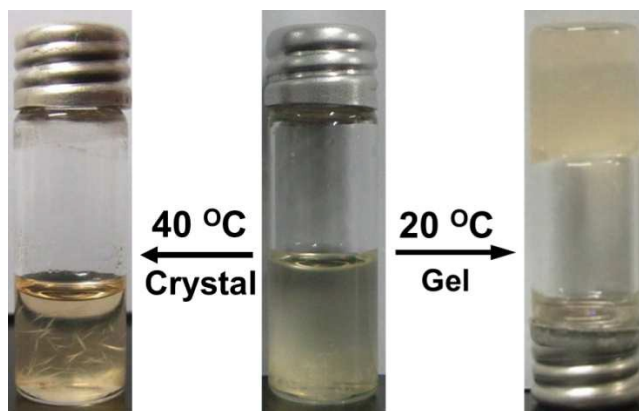
Fig. 1 Photographs of the sol–gel transition (20.0 ^{O}C) and formation of crystalline rods (40.0 ^{O}C) of the POM-cholesterol conjugate (15 mg) in mixed DMF/toluene solvents (v/v = 1:9).

As a consequence of these findings, the samples in mixed DMF/toluene solvents (v/v = 1:9) and toluene were next investigated at different temperatures and concentrations as representatives, to further better understand the influence of temperature on the self-assembly behavior. Typically, sample (15 mg) was dissolved in mixed DMF/toluene solvents (1 mL), and the solution was heated to form a clear solution. Then, it was cooled slowly to 20.0 ^{O}C, and a stable organogel was formed after staying for several hours. Intriguingly, it was maintained at 40.0 ^{O}C and crystal rods were formed in solution after a few weeks. The rods can be seen by the naked eye and their length reaches several millimeters, as shown in Fig. 1. The same phenomenons were achieved only at a concentration range of 8 to 50 mg mL^{-1}, but solutions (c ≤ 8 mg mL^{-1}) or organogels (c ≥ 50 mg mL^{-1}) in mixed DMF/toluene solvents at a mixture ratio of 1/9 in the experiment. In contrast, the sample dissolved in toluene, only formed a stable organogel after a few days or weeks, when it was maintained in a concentration range (c ≥ 5 mg mL^{-1}) at 20.0 ^{O}C or 40.0 ^{O}C. The above studies show that under appropriate conditions, the self-assembly behavior of the POM-cholesterol conjugate in

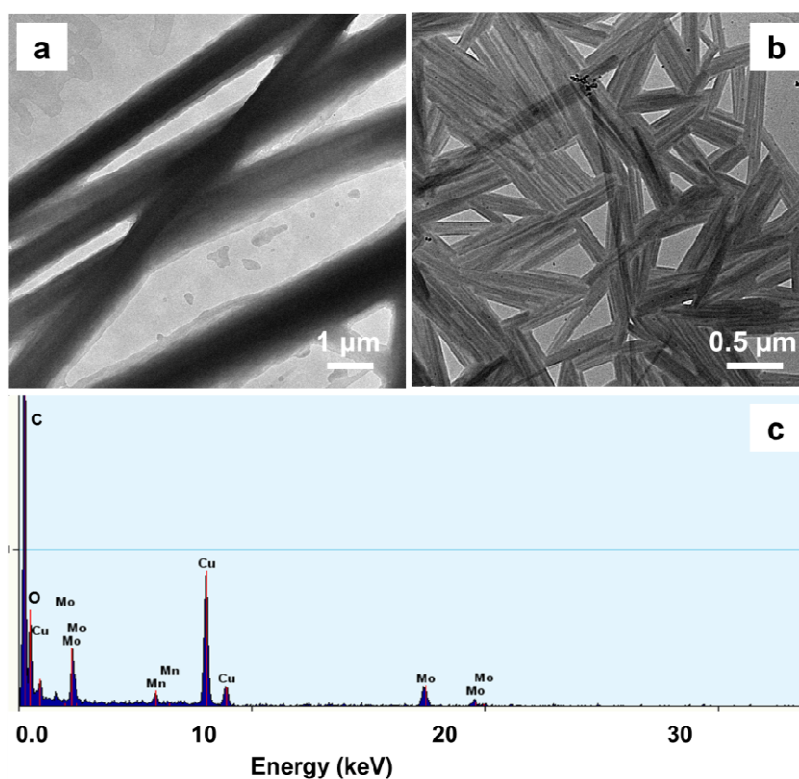mixed DMF/toluene solvents is a temperature-mediated process.

Fig. 2 Supramolecular structure characterizations of the crystalline rods and the dried gel sample (c = 15 mg mL^{-1}). (a) TEM image showing long and rod-like structures; (b) TEM image showing short and elongated structures; (c) EDX spectrum showing characteristic X-ray energies of Mo and Mn existing in the cluster. Note that the Cu peak comes from the copper grid.

Morphology studies

In order to obtain an in-deep insight into the crystal rods and organogel microstructures, the morphological features were directly investigated by TEM studies. For crystal rods, which were constituted in mixed DMF/toluene solvents at 40.0 ^{O}C, it shows a lot of ultralong and rigid rods with a length on micrometer scales and width on nanometer scales, as shown in Fig. 2a, and for organogel, which was formed in mixed DMF/toluene solvents at 20.0 ^{O}C, it exhibits a mass of short and elongated nanoribbons with width ranging from dozens to

hundreds nanometers and length no longer than 3.0 μm, as shown in Fig. 2b. The EDX

spectrum in Fig. 2c indicates the characteristic X-ray energies of Mo and Mn, proving the

existence of the inorganic POM clusters within the crystal rods. However, for organogel,

which was formed in toluene at 20.0 ^{O}C or 40.0 ^{O}C, it shows the same supramolecular

structure, that is a number of similar fibrils with a length longer than 10 μm, and fibrils form
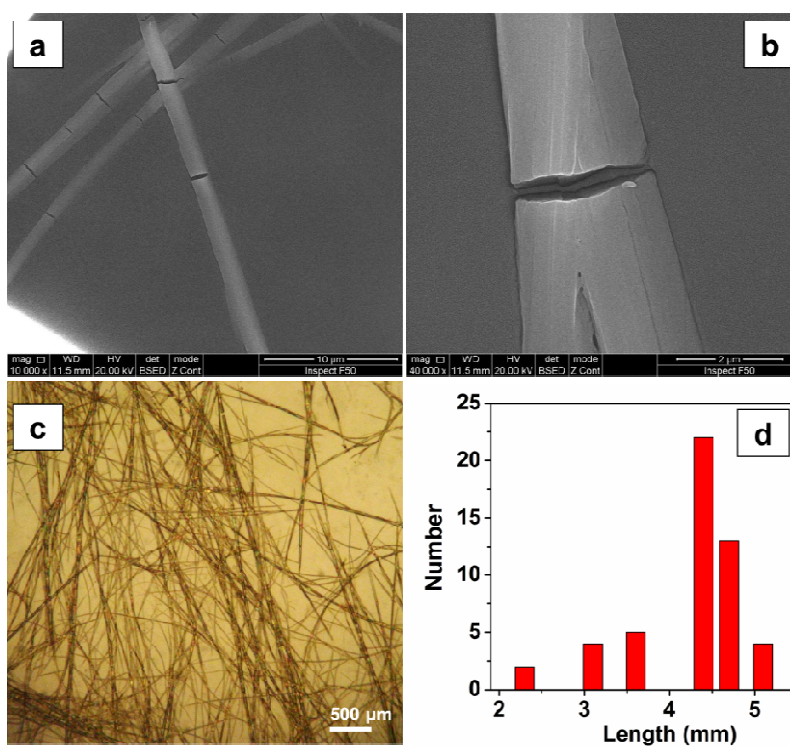
a three-dimensional fibrillar network (see Fig. S3, ESI†).

Fig. 3 Supramolecular structure characterizations of the crystalline rods (c = 15 mg mL^{-1}). (a) SEM image

showing long and rod-like structures; (b) enlarged SEM image showing multilayer structures within a rod;

(c) OM image showing a lot of ultralong and rod-like structures; (d) the statistical analysis of the length.

Since the crystalline rods had relatively large diameters, SEM and optical microscopy

were used to image the aggregation mode. As shown in Fig. 3a–b, examination of the images

clearly reveals that it has rod-like morphology with a width of about 2.0 μm. Similarly, plenty

of ultralong and rod-like aggregates are exhibited on the optical micrograph image, as shown in Fig. 3c. Furthermore, length statistic was analyzed by measuring over 50 microrods in digital photographs. The result in Fig. 3d shows that most of length of the microrods are about 4.4 mm. These results are clearly consistent with the results of TEM studies.
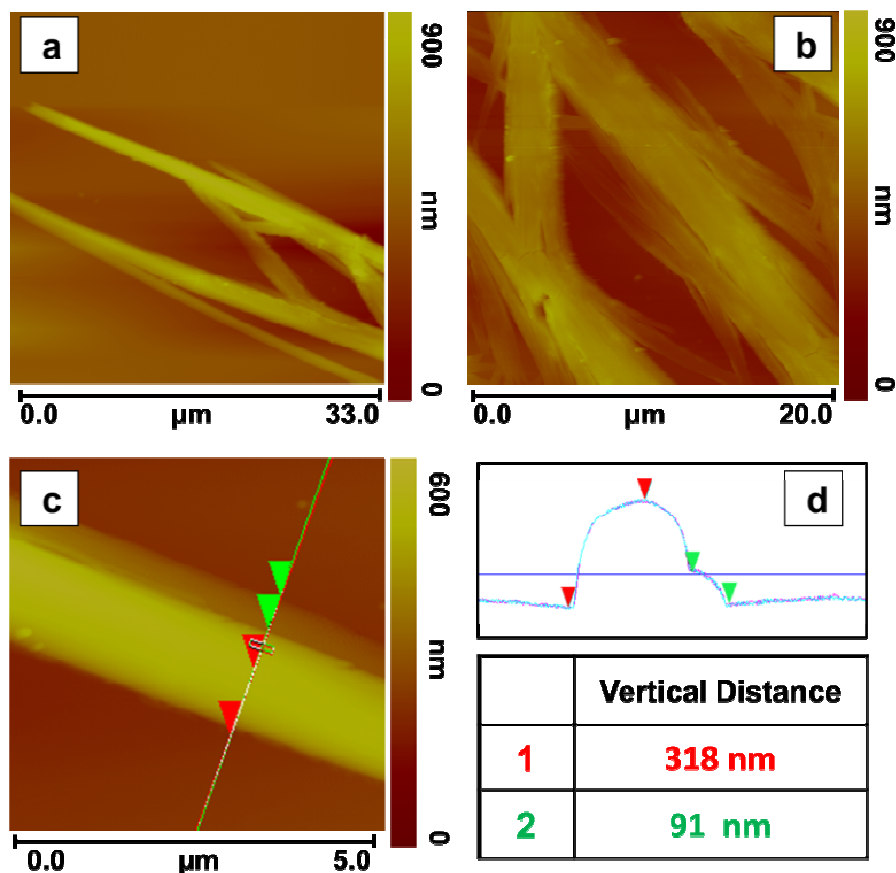

Fig. 4 AFM characterization and analyses of the supramolecular structure in the crystalline rods (c = 15 mg mL^{-1}). (a) AFM height image showing ultralong and rod-like structures; (b) AFM height image showing multilayer structures within rods; (c) further enlarged AFM height image; (d) height profile across the rods showing their height.

In addition, the self-assembly structures of the crystalline rods were also investigated with AFM, shown in Fig. 4a–b, where very long and rod-like structures are observed, indicating that the POM-cholesterol conjugate formed fine structures in mixed DMF/toluene solvents at

40.0 ^{O}C. Also, the AFM images clearly show that the height of the formed microrods is about 90 – 220 nm, and the microrods are hierarchically assembled from several thinner ribs, as shown in Fig. 4c–d. The AFM images are well in agreement with the SEM images and confirm the rod-like morphology.
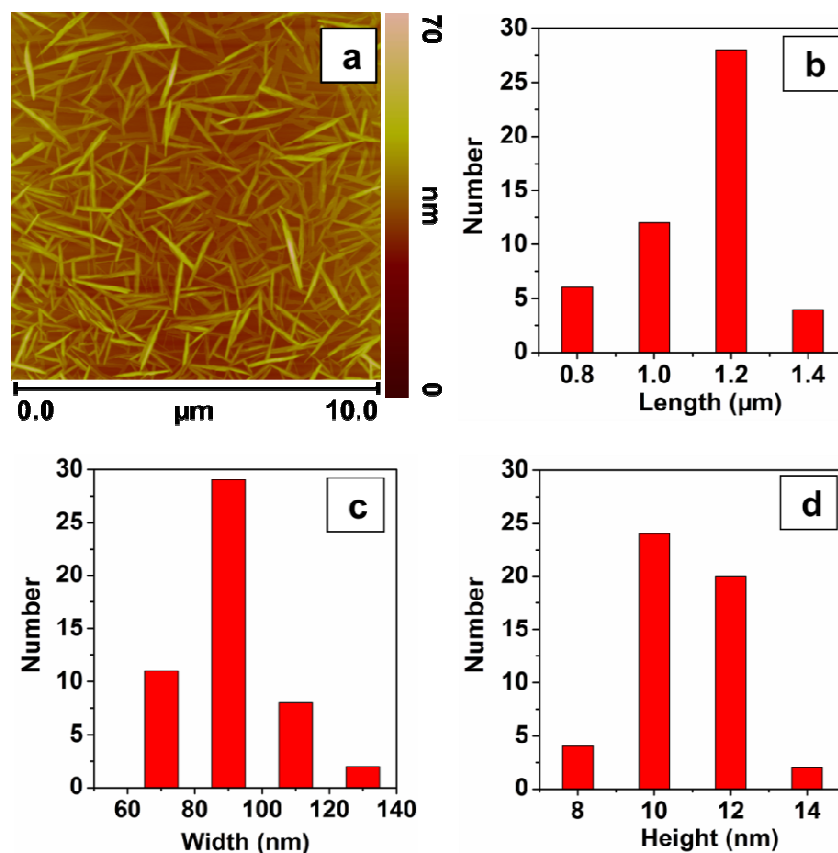

Fig. 5 AFM characterization and analyses of the supramolecular structure in the dried gel sample (c = 15 mg mL^{-1}). (a) AFM height image showing rigid and straight ribbons; (b) the statistical analysis of the length; (c) the statistical analysis of the width; (d) the statistical analysis of the heigth.

Finally, we attempted to understand the self-assembly process of the organogel, and thus aggregate morphologies were investigated using AFM. Fig. 5a shows the AFM image of the organogel in mixed DMF/toluene solvents at 20.0 ^{O}C. The rigid and straight ribbons should

be constructed through the physical connection of the POM-cholesterol conjugates, which immobilize solvent molecules through van der Waals interactions (gelator–solvent interactions) between cholesteryl moieties and solvents, and electrostatic adsorption (gelator–gelator interactions) between POM clusters, resulting in gelation. According to the statistical analysis conducted by measuring over 50 ribbons in AFM image, the ribbons have a length of about 1.2 μm, a width within 60 – 140 nm and a thickness approximately 11.0 nm, as shown in Fig. 5b–d.
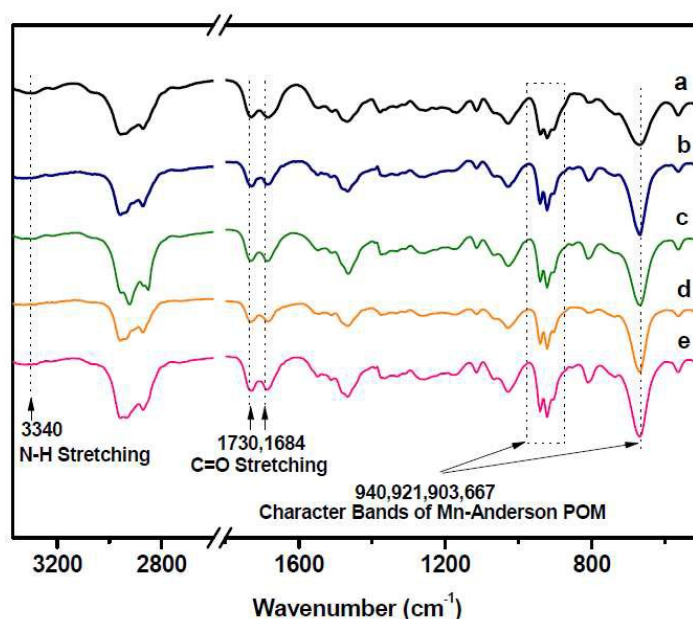

Figure 6 FT-IR spectra of the POM-cholesterol conjugate. (a) original samples; (b) powders of crystalline rods; (c) xerogel in mixed DMF/toluene solvents (v/v = 1:9); (d) xerogel in mixed DMF/toluene solvents (v/v = 1:12) ; (e) xerogel in toluene.

Driving force investigation

To facilitate understanding of the driving force of the crystalline rods and organogel, we carried out a close investigation using FT-IR study, which could offer very helpful information for confirming hydrogen bonding formation. Accordingly, we carried out a

14

variety of measurements, including the powders of original sample, crystalline rods, and xerogels formed in mixed DMF/toluene solvents and toluene, as shown in Fig.6. Obviously, three typical bands corresponding to the stretching vibrations of NH and C = O groups have no shift at all, indicating the hydrogen bonding interactions are not the driving force for the formation of crystalline rods and organogel. Temperature-dependent FT-IR measurement can provide further information of the driving force, and thus the organogels formed in mixed DMF/toluene solvents (v/v = 1:9) and toluene were next studied in detail. It can be seen that the spectra are almost the same, also the stretching vibration of C = O group and bending vibration of NH group have no shift (see Fig. S4, S5, ESI†). Supplementarily, the xerogel in mixed DMF/toluene solvents at a 1/9 ratio were studied with the TGA measurement, and the rapid degradation indicated that the POM-cholesterol conjugate began to decompose at 233 ^{O}C. In other words, the gelator has good thermal stability (see Fig. S6, ESI†).

On the bases of the results obtained from FT-IR and temperature-dependent FT-IR measurements, we suggest that the driving force of self-assembly process are not the hydrogen bonding interactions between the POM-cholesterol conjugates.

X-ray diffraction measurements

It has been well know that XRD is a powerful method in ascertaining detailed structures of the molecular packing.[57] The self-assembled structures of the POM-cholesterol conjugate in the crystalline rods and organogel are respectively reflected by the crystal powder and xerogel sample, whose structural information could be investigated by the XRD analyses. To obtain further insight into the structures of the assemblies, XRD studies were carried out on the quickly vacuum-dried the crystalline rods and organogel.
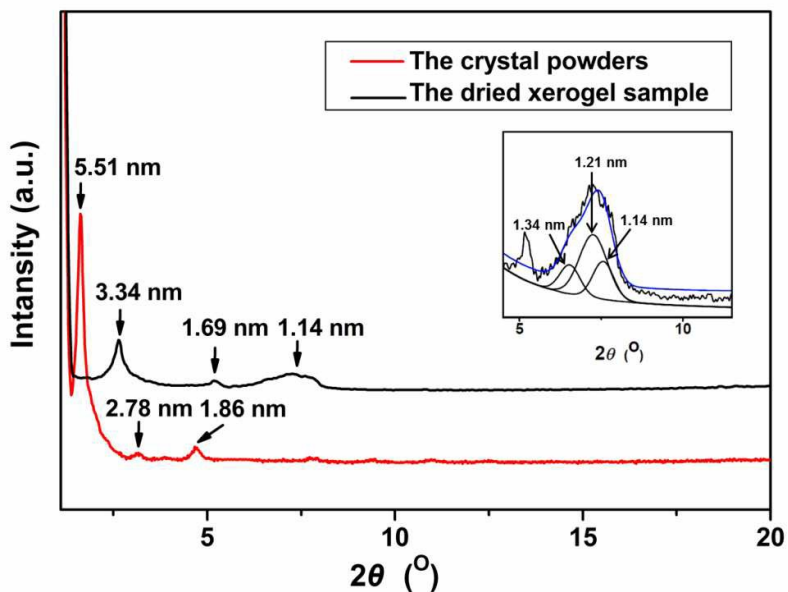
Fig. 7 The XRD pattern and analyses of the crystal powders and xerogel sample (c = 15 mg mL^{-1}). The inset details the XRD pattern of the dried xerogel sample within the $4.5° < 2\theta < 11.5°$.

The XRD patterns of the crystal powders and xerogel sample formed with the POM-cholesterol conjugate are displayed in Fig. 7. The crystal powders exhibit a series of strong diffraction peaks with d-spacings of 5.51, 2.78, and 1.86 nm, and the d-spacing of 5.51 nm is nearly twice of 2.78 nm and triple of 1.86 nm, indicating a lamellar structure with a distance of 5.51 nm. The XRD pattern of the xerogel sample shows relatively broad diffraction peaks with d-spacing $d_1 = 3.34$ nm, $d_2 = 1.69$ nm, and $d_3 = 1.14$ nm, respectively. The ratio of $d_3 : d_2 : d_1 = 1 : 2 : 3$ clearly corresponds to a lamellar structure with an interlamellar spacing of $d = 3.34$ nm. The broad peaks with a peak position at $2\theta \approx 6.5°$ can be split into three sub-peaks. The d-spacing values of 1.34, 1.21 correspond to the POM cluster plus the three tetrabutyl ammonium cations within the ribbons, due to diameter of the pristine POM cluster is 1.2 nm. This suggests that the POM clusters in the organogel arrange slightly disorderly. It is worth mentioning that the d-spacing values of the crystalline rods are

quite different from the organogel. The molecular length of the POM-cholesterol conjugate is calculated with the ChemDraw software (MM2 force field) and Diamond software from the reported crystallographic data (see Fig. S7, ESI†). The molecular length of the POM-cholesterol conjugate is ca. 5.28 nm, close to the interlamellar spacing of $d = 5.51$ nm in the crystalline rods. While, it is much larger than the interlamellar spacing of $d = 3.34$ nm in the organogel. The distinction of the d-spacing values is interpreted as follows: for crystalline rods, the self-assembled structures are constituted with highly ordered and parallel molecules of the POM-cholesterol conjugate, whereas in ribbons of organogel, the layer structures are composed of interdigitating POM layers and cholesterol layers (see Fig. S8, ESI†). This difference implies that the temperature plays an important role in manipulating the self-assembly behavior of the POM-cholesterol conjugate.
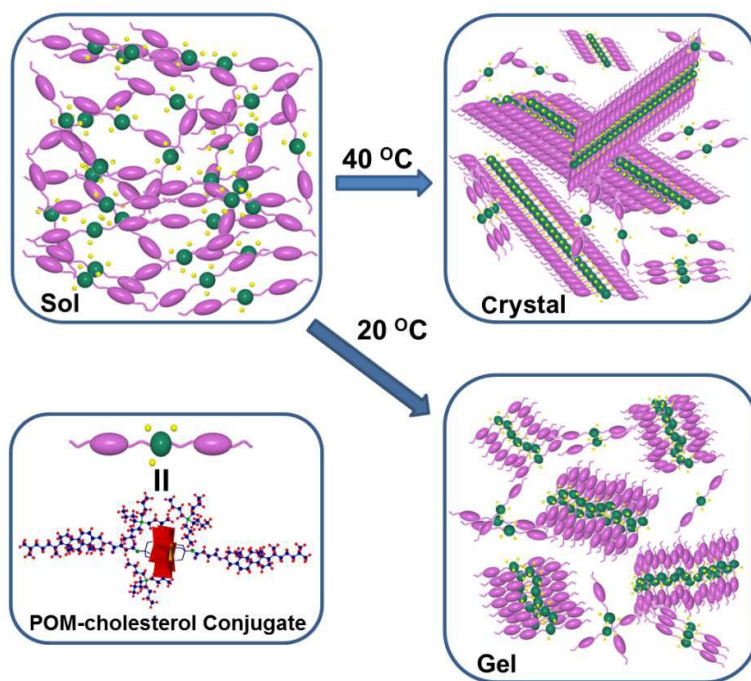
Scheme 2 Schematics represent the different arrangements of the POM-cholesterol conjugate within crystalline rods and nanoribbons.

Discussion on the self-assembly mechanism

On the basis of the above-mentioned results of morphology investigation, we believe that the TEM and SEM studies, especially when supported by AFM studies, have proven undoubtedly that the self-assembly structures of the POM-cholesterol conjugate are highly dependent on the temperature. When we supplement the FT-IR, TGA, XRD data and analyses, we propose a schematic representation to describe the self-assembly process of the POM-cholesterol conjugate in mixed DMF/toluene solvents at different temperatures, as shown in Scheme 2. Because of the different morphology, it is meaningful to have a deep comprehension how the influence of temperature in the self-assembly process of the POM-cholesterol conjugate in mixed DMF/toluene solvents or toluene at 20.0 ^{O}C or 40.0 ^{O}C. As mentioned above, the POM-cholesterol conjugate is consisted of one symmetrical and polar POM cluster and two planar and nonpolar cholesterol moieties. To the best of our knowledge, toluene and DMF is a good solvent for cholesterol moieties and POM cluster, respectively. Specifically, pure toluene has a dielectric constant $\varepsilon^e = 2.24$, and DMF has $\varepsilon^e = 36.71$. The dielectric constant of the mixed solvents is calculated using $\varepsilon^e = \varepsilon^e_{tol} f_{tol} + \varepsilon^e_{DMF} f_{DMF}$, in which ε^e_{tol} and ε^e_{DMF} are the dielectric constants of toluene and DMF, and f_{tol} and f_{DMF} are the volume fraction, respectively. Thus, the mixed DMF/toluene solvents (v/v = 1:9) have a dielectric constant $\varepsilon^e = 5.68$. Our understanding is that the influence of temperature in the self-assembly process of the POM-cholesterol conjugate actually affects the balance between conjugate–conjugate interactions and conjugate–solvent interactions. Specifically, the POM-cholesterol conjugate is heated in mixed DMF/toluene solvents until the solid is dissolved, when the hot solution is cooled and maintained at 40.0 ^{O}C, the molecules start to condense and form ordered

18

aggregates. Note that the dielectric constant of solution is $\varepsilon^e = 5.68$, and the polar POM cluster has good solubility under this condition. In this case, the conjugate–conjugate interactions are slightly greater than conjugate–solvent interactions, due to the strong electrostatic adsorption between the POM clusters is the main driving force. Also, it is well known that POM clusters normally crystallize with a highly ordered structure. As a result, the molecules form ultralong and ordered crystalline rods after a few weeks. Meanwhile, the formation of crystalline rods needs such a long time, this phenomenon reflects that the self-assembly progress of molecules is very slow, namely the conjugate–conjugate interactions are only slightly greater than conjugate–solvent interactions at 40.0 ^{O}C.

On the contrary, when the hot solution of the POM-cholesterol conjugate is gradually cooled and maintained at 20.0 ^{O}C, the solubility of the POM clusters in the mixed solvents is obviously decreased, and thus this variation weakens electrostatic adsorption between the POM clusters. Namely, the decrease of temperature weakens the conjugate–conjugate interactions but strengthens the solvent–gelator interactions. Finally, a delicate balance is kept between the conjugate–conjugate interactions and conjugate–solvent interactions at 20.0 ^{O}C. As a consequence, the molecules assemble into nanoribbons, and thus solution of the POM-cholesterol conjugate becomes immobilized like a solid after several hours. Apparently, compared with the formation of crystalline rods, the gelation rate is increased because of the balance of conjugate–conjugate interactions and solvent–gelator interactions.

For the self-assembly process of the POM-cholesterol conjugate in toluene, the dielectric constant of solution is $\varepsilon^e = 2.24$, and the POM cluster is almost insoluble, while the cholesterol moieties on the two sides of the POM cluster is very soluble. The dissolution of

the POM-cholesterol conjugate in toluene at a high temperature is attributed to the interactions between two cholesterol moieties and toluene molecules, namely the conjugate–solvent interactions. When the hot solution is cooled to 40.0 ^{O}C or 20.0 ^{O}C, the solubility of the POM-cholesterol conjugate is decreased, and thus the conjugate–solvent interactions is weakened. The molecules slowly assemble into fibrils because of the poor solubility of the POM cluster in toluene plus interactions between cholesterol moieties and toluene molecules. Once the balance is formed between conjugate–conjugate interactions and conjugate–solvent interactions, the solution eventually becomes immobilized. Note that the gelation process takes a long time, this is due to the poor solubility of the POM cluster in toluene.

In the previous subsection of the XRD analyses, we mentioned an intriguing phenomenon that the *d*-spacing values of the crystalline rods are quite different from the organogel, and two self-assembled structure models are suggested. Our interpretation is as follows: for crystalline rods, the strong electrostatic adsorption between the POM clusters is the main driving force, the formation of the highly ordered and parallel structure of the POM-cholesterol conjugate can maximize the interactions between the POM clusters as well as conjugate–conjugate interactions. For the ribbons in the organogel, the interactions between the POM clusters are weakened, but the conjugate–solvent interactions are strengthened, plus the well-known fact that cholesterol moieties aggregated via van der Waals interactions between molecules, thus the self-assembled structures are constituted with an alternately arranged POM layers and cholesterol layers, and have a slightly disorderly structure, which is reflected by the two sub-peaks with a peak position at $2\theta \approx 6.5°$.

Finally, we concern the influence of different concentrations of the POM-cholesterol conjugate and solvents on the self-assembly behavior. The samples at a concentration range of 8 to 50 mg mL^{-1} can be well controlled and regulated to form crystalline rods or organogels in the mixed DMF/toluene solvents at a 1/9 ratio by means of temperature-mediated approach. Our interpretation is that the interactions (*e.g.* conjugate–conjugate interactions, conjugate–solvent interactions) between POM-cholesterol conjugates and solvents are regulated with the dielectric constant of solvent and solubility of the POM cluster, which are also determined by the temperature. When the hot solution of the POM-cholesterol conjugate is cooled, the molecules start to condense and three situations are possible: (1) the conjugate–conjugate interactions are slightly greater than conjugate–solvent interactions, leading to a highly ordered assembly giving rise to crystalline rods, (2) the conjugate–conjugate interactions are weaker than conjugate–solvent interactions, resulting in a solution, or (3) a delicate balance between conjugate–conjugate interactions and conjugate–solvent interactions, yielding an organogel. Only when concentrations of the POM-cholesterol conjugate and solvents make the interactions between POM-cholesterol conjugates and solvents respectively correspond to the first situation and third situation at the different temperature, do the self-assembly of polyoxometalate-cholesterol conjugate can be well controlled and regulated by the temperature.

Conclusions

In summary, we have profoundly investigated the influence of temperature on the polyoxometalate-based self-assembly behavior and successfully demonstrated that the self-assembly of the polyoxometalate-cholesterol conjugate can be well controlled and

regulated by means of temperature-mediated approach. Utilizing this approach, the polyoxometalate-cholesterol conjugate assembled into ultralong and rigid microrods at 40.0 ^{O}C, and an elongated nanoribbons at 20.0 ^{O}C, in mixed DMF/toluene solvents (v/v = 1:9). Moreover, a mechanism has been proposed to explain the self-assembly behavior of the polyoxometalate-cholesterol conjugate at 40.0 ^{O}C and 20.0 ^{O}C. Therefore, the results described herein may provide a feasible method for the fabrication of nanostructural materials for various applications.
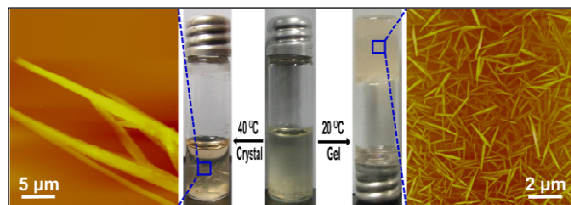
Acknowledgements

References

1 N. M. Sangeetha, U. Maitra, *Chem. Soc. Rev.*, 2005, **34**, 821–836.

2 P. Dastidar, *Chem. Soc. Rev.*, 2008, **37**, 2699–2715.

3 C. X. Fan, H. B. Qiu, J. F. Ruan, O. Terasaki, Y. Yan, Z. X. Wei and S. Che, *Adv. Funct. Mater.*, 2008, **18**, 2699–2707.

4 L. Ziserman, H. Y. Lee, S. R. Raghavan, A. Mor and D. Danino, *J. Am. Chem. Soc.*, 2011, **133**, 2511–2517.

5 A. Ajayaghosh, V. K. Praveen and C. Vijayakumar, *Chem. Soc. Rev.*, 2008, **37**, 109–122.

6 S. Zhang, S. Yang, J. Zang, R. Yang, G. Zhao and C. Xu, *Chem. Commun.*, 2014, **69**,

9943–9946.

7 X. J. Wang, L. B. Xing, W. N. Cao, X. B. Li, B. Chen, C. H. Tung, L. Z. Wu, *Langmuir*, 2011, **27**, 774–781.

8 J. Peng, F.Zhai, X. Y.Guo, X. P. Jiang and Y. G. Ma, *RSC Adv.*, 2014, **4**, 13078–13084.

9 Y. Y.Wang, D. Y. Zhou, H. N. Li, R. R. Li, Y. Y. Zhong, X. Sun and X. Sun, *J. Mater. Chem. C*, 2014, **2**, 6402–6409.

10 M. Prehm, X. H. Cheng, S. Diele, M. K. Das and C. Tschierske, *J. Am. Chem. Soc.*, 2002, **124**, 12072–12073.

11 C. Keith, R. A. Reddy, U. Baumeister and C. Tschierske, *J. Am. Chem. Soc.*, 2004, **126**, 14312–14313.

12 R. de la Rica and H. Matsui, *Chem. Soc. Rev.*, 2010, **39**, 3499–3509.

13 P. C. Xue, R. Lu, X. C. Yang, L. Zhao, D. F. Xu, Y. Liu, H. Z. Zhang, H. Nomoto, M. Takafuji and H. Ihara, *Chem. Eur. J.*, 2009, **15**, 9824–9835.

14 C. Wang, Q. Chen, F. Sun, D. Q Zhang, G. X. Zhang,Y. Y. Huang, R. Zhao and D. B. Zhu, *J. Am. Chem. Soc.*, 2010, **132**, 3092–3096.

15 S. Sumiya,Y. Shiraishiand, T. Hirai, *New J. Chem.*, 2013, **37**, 2642–2647.

16 Polyoxometalate chemistry–from topology via self-assembly to applications, ed. M. T. Pope and A. Müller, Kluwer Academic Publishers, *Dordrecht*, 2001.

17 D. L. Long, R. Tsunashima and L. Cronin, *Angew. Chem. Int. Ed.*, 2010, **49**, 1736–1758.

18 Y. Yan and L. X. Wu, *Isr. J. Chem.*, 2011, **51**, 181–190.

19 A. Proust, B. Matt, R. Villanneau, G. Guillemot, P. Gouzerhand G. Izzet, *Chem. Soc. Rev.*, 2012, **41**, 7605–7622.

20 A. Proust, R Thouvenot and P. Gouzerh, *Chem. Commun.*, 2008, 1837–1852.

21 Y. Kikukawa, Y. Kuroda, K. Yamaguchi and N. Mizuno, *Angew. Chem. Int. Ed.*, 2012, **51**, 2434–2437.

22 S. Y. Yin, H. Sun, Y. Yan, W. Li and L. X. Wu, *J. Phys. Chem. B*, 2009, **113**, 2355–2364.

23 S. Favette, B. Hasenknopf, J. Vaissermann, P. Gouzerh and C. Roux, *Chem.Commun.*, 2003, 2664–2665.

24 M. Speldrich, H. Schilder, H. Lueken and P. Kögerler, *Isr. Chem.*, 2011, **51**, 215–227.

25 B. Matt, C. Coudret, C. Viala, D. Jouvenot, F. Loiseau, G. Izzet and A. Proust, *Inorg. Chem.*, 2011, **50**, 7761–7768.

26 E. Cartuyvels; K. Van Hecke; L. Van Meervelt; C. Görller-Walrand;T. N.Parac-Vogt, *J. Inorg. Biochem.*, 2008, **102**, 1589–1598.

27 X. H. Yan, P. L. Zhu, J. B. Fei and J. B. Li, *Adv. Mater.*, 2010, **22**, 1283–1287.

28 G. Geisberger; S. Paulus; E. B. Gyenge; C. Maake; G. R. Patzke, *Small*, 2011, **7**, 2808–2814.

29 M. H. Rosnes, C. Musumeci, C. P. Pradeep, J. S. Mathieson, D. L. Long, Y. F. Song, B. Pignataro, R. Cogdell and L. Cronin, *J. Am. Chem. Soc.*, 2010, **132**, 15490–15492.

30 M. P. Santoni, A. K. Pal, G. S. Hanan, M. C. Tang, K. Venne, A. Furtos, P. M. Tremblay, C. Malveau and B. Hasenknopf, *Chem. Commun.*, 2012, **48**, 200–202.

31 Y. Yan, H. B. Wang, B. Li, G. F. Hou, Z. D. Yin, L. X. Wu and V. W. W. Yam, *Angew. Chem. Int. Ed.*, 2010, **49**, 9233–9236.

32 J. Zhang, W. Li, C. Wu, B. Li, J. Zhang and L. X. Wu, *Chem. Eur. J.*, 2013, **19**, 8129–8135.

33 Z. F. He, B. Li, H. Ai, H. L. Li and L. X. Wu, *Chem. Commun.*, 2013, **49**, 8039–8041.

34 B. Zhang, L. Yue, Y. Wang, Y. Yang and L. X. Wu, *Chem. Commun.*, 2014, **50**, 10823–10826.

35 J. Schulz, R. Gyepes, I. Císařová and P. Štěpnička, *New J. Chem.*, 2010, **34**, 2749–2756.

36 Y. Yan, B. Li, Q. Y. He, Z. F. He, H. Ai, H. B. Wang, Z. D. Yin and L. X. Wu, *Soft Matter*, 2012, **8**, 1593–1600.

37 J. Zhang, Y. F. Song, L. Cronin and T. B. Liu, *J. Am. Chem. Soc.*, 2008, **130**, 14408–14409.

38 Y. F. Song, N. McMillan, D. L. Long, J. Thiel, Y. L. Ding, H. S. Chen, N. Gadegaard and L. Cronin, *Chem. Eur. J.*, 2008, **14**, 2349–2354.

39 D. Schaming, C. Allain, R. Farha, M. Goldmann, S. Lobstein, A. Giraudeau, B. Hasenknopf and L. Ruhlmann, *Langmuir*, 2010, **26**, 5101–5109.

40 C. Allain, D. Schaming, N. Karakostas, M. Erard, J. P. Gisselbrecht, S. Sorgues, I. Lampre, L. Ruhlmann and B. Hasenknopf, *DaltonTrans.*, 2013, **42**, 2745–2754.

41 S. Nlatelv, L. Plaultl and D. Astruc, *Chem. Eur. J.*, 2006, **12**, 903–914.

42 Y. L. Wang, X. L. Wang, X. J. Zhang, N. Xia, B. Liu, J. Yang, W. Yu, M. B. Hu, M. Yang and W. Wang, *Chem. Eur. J.*, 2010, **16**, 12545–12548.

43 B. Liu, J. Yang, M. Yang, Y. L. Wang, N. Xia, Z. J. Zhang, P. Zheng, W. Wang, I. Lieberwirth and C. Kübel, *Soft Matter*, 2011, **7**, 2317–2320.

44 M. B. Hu, Z. Y.Hou, W. Q.Hao, Y. Xiao, W. Yu, C. Ma, L. J. Ren, P. Zheng and W. Wang, *Langmuir*, 2013, **29**, 5714–5722.

45 Y. Leng, J. W. Zhao, P. P. Jiang and J. Wang, *RSC Adv.*, 2015, **5**, 17709–17715.

46 H. B. Wang, Y. Yan, B. Li, L. H. Bi and L. X. Wu, *Chem. Eur. J.*, 2011, **17**, 4273–4282.

47 H. B. Wang, Y. Yan, B. Li, L. H. Bi and L. X. Wu, *Soft Matter*, 2012, **8**, 3315–3321.

48 M. F. Misdrahi, M. H. Wang, C. P. Pradeep, F. Y. Li, C. Lydon, L. Xu, L. Cronin and T. B. Liu, *Langmuir*, 2011, **27**, 9193–9202.

49 A. Nisar, X. X. Xu, S. L. Shen, S. Hu and X. Wang, *Adv. Funct. Mater.*, 2009, **19**, 860–865.

50 Y. F. Wang and I. A. Weinstock, *Chem. Soc. Rev.*, 2012, **41**, 7479–7496.

51 A. Nisar, J. Zhuang and X. Wang, *Chem. Mater.*, 2009, **21**, 3745–3751.

52 D Li, J. Song, P. C. Yin, S. Simotwo, A. J. Bassler, Y. Y. Aung, J. E. Roberts, K. I. Hardcastle, C. L. Hill and T. B. Liu, *J. Am. Chem. Soc.*, 2011, **133**, 14010–14016.

53 M. M. Su, H. K. Yang, L. J. Ren, P. Zheng and W. Wang, *Soft Matter*, 2015, 11, 741–748.

54 M. M. Su, H. K. Yang, L. J. Ren, P. Zheng and W. Wang, *DaltonTrans.*, 2012, **41**,10043–10051.

55 P. R. Marcoux, B. Hasenknopf, J. Vaissermann and P. Gouzerh, *Eur. J. Inorg. Chem.*, 2003, 2406–2412.

56 H. K. Yang, Y. X. Cheng, M. M. Su, Y. Xiao, M. B. Hu, W. Wang and Q. Wang, *Bioorg. Med. Lett.*, 2013, **23**, 1381–1389.

57 T. Kato, *Angew. Chem. Int. Ed.*, 2010, **49**, 7847–7848.

The self-assembly of the polyoxometalate-cholesterol conjugate can be well controlled and regulated by means of temperature-mediated approach.